Microstructure and mechanical properties of doped-lanthanum gallate with addition of yttria-stabilized zirconia

T. G. Fujimoto[1]*, V. Seriacopi[2,3], I. F. Machado[2], E. N. S. Muccillo[1]
[1]IPEN, Center of Materials Science and Technology, 055508-000, São Paulo, SP, Brazil
[2]Universidade de São Paulo, Escola Politécnica, São Paulo, SP, Brazil
[3]Maua Institute of Technology, Mechanical Engineering Department, 09580-900, São Caetano do Sul, SP, Brazil

Abstract

Strontium- and magnesium-doped lanthanum gallate ceramics exhibiting relatively high values of ionic conductivity, and chemical stability over a wide range of oxygen partial pressure are considered potential solid electrolytes for application in electrochemical devices for clean energy production. Recently, the addition of a second phase has been a strategy to improve the performance of solid electrolytes. In this work, doped-lanthanum gallate ceramics with up to 20 wt% yttria-stabilized zirconia addition were investigated to determine the effects of the minor phase on the microstructure evolution, hardness, and elastic modulus of the matrix. Composite solid electrolytes were prepared by mechanical mixing followed by solid-state sintering in the 1350-1500 ºC range. The mean grain size of composites was lower than that of the matrix for sintering temperatures up to 1400 ºC, but a fast grain growth was observed for higher temperatures. Improved mechanical properties were obtained for composites compared to those of the matrix.
Keywords: solid electrolyte, microstructure, nanoindentation.

INTRODUCTION

Polycrystalline ceramics with perovskite structure based on lanthanum gallate with partial substitution in the A and B sites for strontium and magnesium, respectively, are well-known oxide ion conductors with potential application in solid oxide fuel cells (SOFCs) for clean-energy production [1-3]. Attributes such as high ionic conductivity, transference number of approximately 1 over a wide range of oxygen partial pressures (0.4 to 10^{-24} atm at 800 ºC), and good stability during long-term operation, turn this ceramic solid electrolyte as an alternative for SOFCs operating in the intermediate-temperature range (~550 to 750 ºC) [2, 3]. In general, doped lanthanum gallates are not single-phase ceramics and randomly distributed impurity phases such as $LaSrGaO_4$, $La_4Ga_2O_9$, and $LaSrGa_3O_7$, along with MgO precipitated at the grain boundaries are usually found [4-6]. The $La_{0.9}Sr_{0.1}Ga_{0.8}Mg_{0.2}O_{3-\delta}$ composition, hereafter LSGM, with orthorhombic symmetry, besides high ionic conductivity (0.127 S.cm^{-1} at 800 ºC), shows a relatively low fraction of impurity phases compared to other compositions [7].

Over the last years, increasing attention has been given to composite electrolytes, aiming to improve their overall performance [8-15]. The addition of a second electrolyte may bring about improvements in several properties of the major phase, such as increased densification [12], improved microstructural homogeneity [8], enhanced mechanical properties [9, 11], decrease of the grain boundary resistivity [10], increase of the total ionic conductivity [13, 14], and

lowering of the area specific resistance of SOFCs [15]. Relatively few studies involving LSGM as the major phase may be found [16-20]. Composites consisting of $La_{0.85}Sr_{0.15}Ga_{0.8}Mg_{0.2}O_{2.825}$ (LSGM1520)-x$Ce_{0.85}Sm_{0.15}O_{1.925}$ (SDC15) with x= 2, 5, 7, and 10 wt% sintered at 1450 ºC for 5 h showed that the minor phase is located at triple grain junctions. The mean grain size decreased with an increasing fraction of SDC15. The thermal expansion coefficients of LSGM1520 and composites ranged from 10.5x10^{-6} to 12x10^{-6} ºC^{-1} at 200 to 600 ºC, and the ionic conductivity was higher for pure material (LSGM1520) [16]. Composites of LSGM-x$Ce_{0.8}Gd_{0.2}O_{1.9}$ (GDC20), with x= 5, 10, and 20 wt% were prepared by the solid-state reaction method and sintered at 1450 ºC for 15 h. A decrease in the mean grain size was observed with increasing the fraction of GDC20. The microstructure of sintered specimens also evidenced MgO precipitated at grain boundaries. For temperatures below approximately 600 ºC, pure LSGM exhibited higher ionic conductivity than composites, whereas, for higher temperatures, the composite with 5 wt% GDC20 displayed the highest conductivity [17]. Composites of LSGM-x$La_{1.55}Sr_{0.45}Ga_3O_{7+\delta}$ (LSG) with x= 1 and 5 wt% were synthesized by the solid-state reaction method and sintered at 1450 ºC for 4 h. The sintered density and the ionic conductivity increased with an increasing fraction of LSG. The mean grain size varied from 5.5 to 6.7 μm, and the extension of the electrolytic domain did not change up to 700 ºC [18]. Chemically synthesized composites of LSGM-10 wt% $Ce_{0.85}Sm_{0.15}O_{1.925}$ (SDC15) were sintered at mild conditions of 1300 ºC for 4 h. The sintered density varied from 88% to 92% of the theoretical value, and $Sm_3Ga_5O_{12}$ was detected as an impurity phase. In the 500 to 700 ºC range, the ionic conductivity of the composite was higher

*talita.fujimoto@usp.br
https://orcid.org/0000-0003-3932-4582

than those of pure LSGM and SDC15 solid electrolytes [19]. In a previous study, it was shown that the addition of a small fraction of 8 mol% yttria-stabilized zirconia (8YSZ) to LSGM produced a small although unexpected increase in ionic conductivity [20]. In this work, microstructure features and mechanical properties determined by indentation tests are focused on aiming to obtain a full account of the effects of 8YSZ addition to LSGM.

EXPERIMENTAL

The starting materials were lanthanum oxide (La_2O_3, Alfa Aesar, 99.9%), gallium oxide (Ga_2O_3, Alfa Aesar, 99.99%), strontium carbonate ($SrCO_3$, Alfa Aesar, 99.99%) and magnesium oxide (MgO, Merck, R.G.). The $La_{0.9}Sr_{0.1}Ga_{0.8}Mg_{0.2}O_{3-\delta}$ solid electrolyte was prepared by the solid-state reaction method, as described elsewhere [21]. Commercial 8 mol% yttria-stabilized zirconia (8YSZ, Tosoh, 99.6%) was used as the minor phase to prepare composite electrolytes of (100-x)LSGM-x8YSZ, with x= 1, 10, and 20 wt%. The composites were obtained by weighing in nominal proportions the synthesized LSGM and 8YSZ, after drying in an oven overnight at 100 ºC. The mixtures were homogenized in agate mortar with a pestle with isopropyl alcohol until drying and stored in an oven at 100 ºC before pressing. The mixtures were pressed (Z2T, Kratos) into pellets (ϕ 9 mm and thickness of 3 mm) in a stainless steel die. Sintering experiments were carried out in a resistive furnace (BlueM, Lindberg) in the 1350 to 1500 ºC range with 4 h holding time and 10 ºC.min⁻¹ heating and cooling rates. Hereafter, the composites are named according to the content of the minor phase as 8YSZ1, 8YSZ10, and 8YSZ20 for x= 1, 10, and 20 wt%, respectively.

Structural analysis of sintered pellets was carried out by X-ray diffraction, XRD (D8 Advance, Bruker-AXS), in the 20º≤2θ≤80º range with 0.05º step size and 2 s counting time per step, 40 kV, and 30 mA and with CuKα (λ=1.5405 Å) radiation. Microstructure evolution was evaluated by field emission gun scanning electron microscopy, FEG-SEM (Inspect F50, FEI) with secondary electrons, on the polished and thermally etched surface of specimens. The mean grain size was estimated by the intercept method with ImageJ software. Microstructure images were also obtained with backscattered electrons (JSM6701F, Jeol) followed by energy dispersive spectroscopy, EDS, on selected microregions. The electrochemical impedance spectroscopy technique was utilized for electrical conductivity measurements using an LF analyzer (4192A, HP) in the 5 Hz to 13 MHz range with 200 mV of applied signal. Silver electrodes were applied by painting followed by curing for this analysis. The impedance spectra were deconvoluted with special software [22]. Nanoindentation tests were performed with a triboindenter (Hysitron TI 950, Bruker) under load of 8 mN, with loading, holding, and unloading stages of 5 s each. Diamond indenter with Berkovich geometry was applied during tests. Load-displacement curves (P-h curves) were obtained. The reduced modulus and the indentation hardness

have been predicted by data analysis using the Oliver-Pharr algorithm [23].

RESULTS AND DISCUSSION

The XRD patterns recorded after sintering at several temperatures exhibited similar features. Fig. 1 depicts, as an example, the XRD patterns of LSGM, 8YSZ, and composites sintered at 1350 ºC. The XRD profiles of pure ceramics were indexed according to PDF 51-290 (LSGM) and 30-1468 (8YSZ) with orthorhombic and cubic symmetries, respectively. The XRD profile of the 8YSZ10 composite was similar to that of LSGM, except for a slight shift of the diffraction peaks to lower angles. This effect indicated some degree of solubility of the minor phase (8YSZ) into the matrix (LSGM). The high-intensity diffraction peaks of the minor phase are identified in the 8YSZ20 pattern by Δ. The diffraction pattern of 8YSZ20 also shows some peaks (marked with *) attributed to lanthanum zirconate, $La_2Zr_2O_7$ (PDF 73-444), with pyrochlore structure as impurity phase. Although the impurity phase was not detected by XRD in the 8YSZ10 composite, its formation may not be discarded.
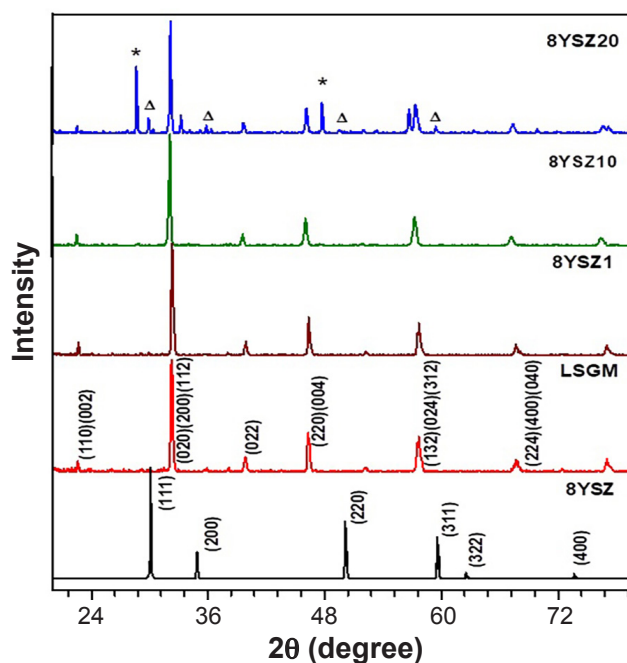

Figure 1: XRD patterns of pure LSGM and 8YSZ, and composites sintered at 1350 ºC for 4 h.

Fig. 2 shows FEG-SEM micrographs of 8YSZ1 composite sintered at 1350, 1400, and 1450 ºC. The grains were polygonal in shape and the major part of the porosity disappeared after sintering at 1400 ºC. The surface of the grains was either smooth or rough. The different textures of grains are usually observed in pure LSGM and seem to be related to lattice defects [6, 24]. The distribution of grain sizes is relatively wide, especially for specimens sintered at high temperatures. The evolution of the mean grain size of
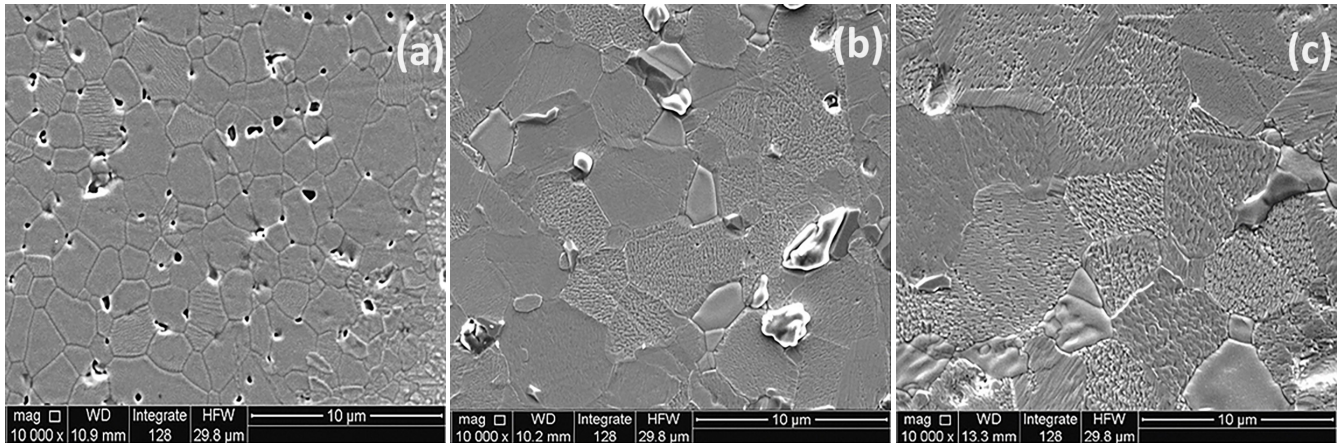
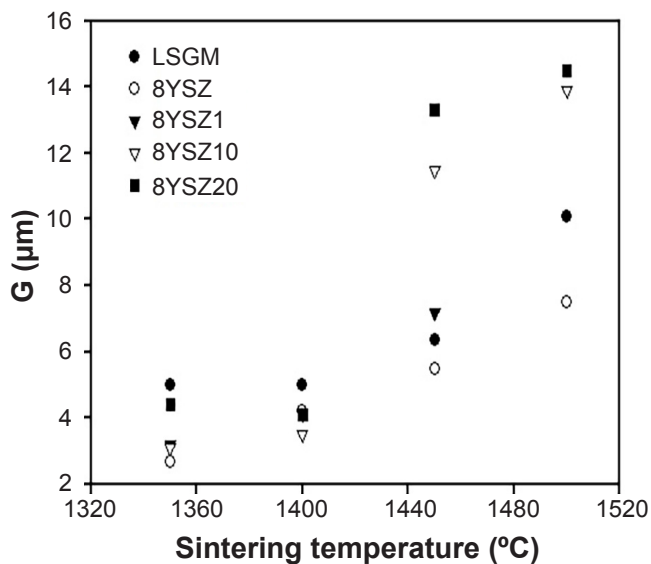Figure 2: FEG-SEM micrographs of 8YSZ1 composite sintered at: a) 1350 ºC; b) 1400 ºC; and c) 1450 ºC.

Figure 3: Evolution of the mean grain size, G, of pure LSGM and 8YSZ1, 8YSZ10, and 8YSZ20 composites with the sintering temperature.

pure ceramics and composites with the sintering temperature is depicted in Fig. 3. At any temperature, the mean grain size of 8YSZ was lower than that of LSGM. The grain sizes of composites were also smaller than that of LSGM up to 1400 ºC. This effect may be a consequence of the smaller grain size of 8YSZ, and possibly a hindering of the grain growth process produced by the minor phase at the grain boundaries and triple grain junctions. For sintering temperatures higher than 1400 ºC, a reverse trend occurred with composites showing higher grain sizes than LSGM. The grain growth of the 8YSZ1 composite with the sintering temperature was similar to that of the matrix, as expected, due to the small fraction of the minor phase. The fast increase of the mean grain size of 8YSZ10 and 8YSZ20 composites at high temperatures seemed to be related to the solubility of the minor phase into LSGM, and the formation of the pyrochlore impurity phase (Fig. 1).

It is well-known that pores may have a deleterious effect on the electrical conductivity of solid electrolytes

[25]. Then, it was shown in a previous work that electrical conductivity data for specimens sintered at 1450 ºC, because of the high density achieved by composites as well as pure ceramics at that temperature [20]. The grain size influences the electrical conductivity of grain boundaries and interfaces, but no evidence was found concerning its effect on the bulk conductivity. This is shown by the Arrhenius plots of the bulk conductivity of 8YSZ10 sintered at 1400 and 1450 ºC (Fig. 4). In the limited temperature range of measurements, both composites exhibited a single straight line with an activation energy of 0.86±0.05 eV (1400 ºC) and 0.93±0.05 eV (1450 ºC). At the lowest temperatures of measurements (~250 to 300 ºC), the bulk electrical conductivity of both specimens was similar. Nevertheless, for higher temperatures, the specimen sintered at 1450 ºC exhibited higher electrical conductivity. This difference in the activation energy for conduction suggested a deviation from the stoichiometry of the matrix. In what follows, experimental results obtained for specimens sintered at 1450 ºC are focused.
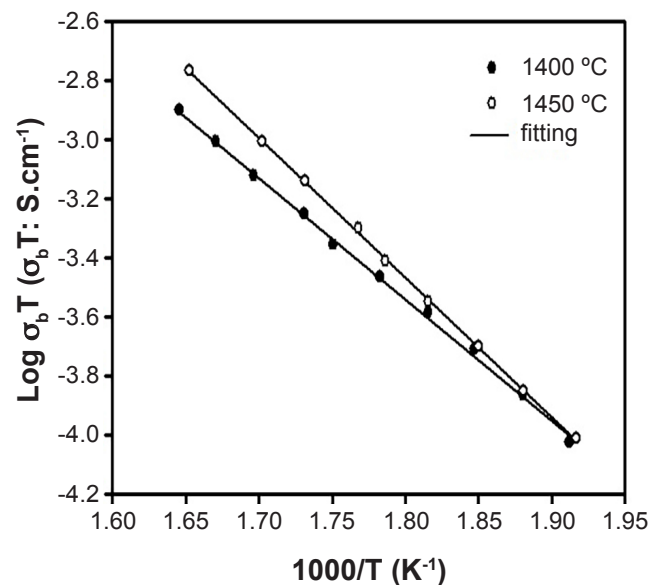

Figure 4: Arrhenius plots of the bulk conductivity of 8YSZ1 composite with the sintering temperature.
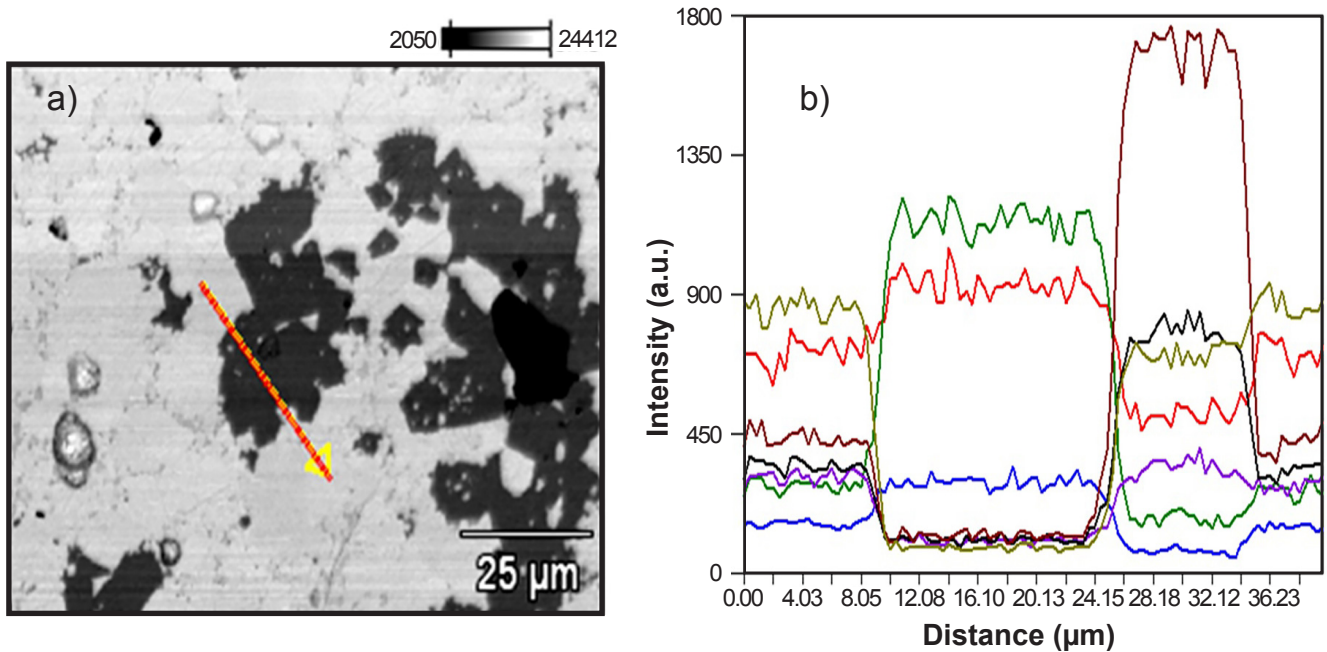
Figure 5: Backscattered electron image-SEM (a) and results of line scan obtained by EDS of a selected microregion (b) of 8YSZ10 composite sintered at 1450 ºC (line color: La: yellow, Sr: purple, Ga: blue, Mg: green, Zr: brown, Y: black, O: red).

Fig. 5a shows a FEG-SEM micrograph (backscattered electron image) and Fig. 5b shows the results of a line scan profile obtained by EDS in LSGM10 composite. In the micrograph, an arrow identifies the selected microregion for analysis and its path for the elemental line scan. The dark microregion was preferentially constituted by Mg (green line). In the same area, a small increase in the counts of Ga (blue line) evidenced an enrichment of this element along with oxygen (red line) and Mg leading to impurity phases. This enrichment of gallium and oxygen at grain boundaries may account for the loss of gallium in the bulk during sintering at high temperatures [26]. In the sequence, a huge increase of the signals of Zr (brown line) and Y (black line) was found, indicating an 8YSZ grain. The profile at both extremes was similar and corresponded to that of the matrix.

Values of the reduced elastic modulus (REM) and hardness obtained from nanoindentation tests are summarized in Table I. The minor phase was harder than LSGM. In addition, the reduced modulus was also higher for 8YSZ. The 8YSZ10 composite exhibited intermediate values of REM and hardness compared to those of 8YSZ and LSGM. Increasing the fraction of 8YSZ in the composite, two distinct behaviors were observed on the load-displacement curve, denoted in Table I as hard and soft phases. The soft phase showed slightly lower hardness than that of 8YSZ-10, but higher REM. The hardness of the hard phase was similar to that of LSGM10, although the REM was higher than those of LSGM, 8YSZ, and 8YSZ10. Despite the complex microstructural development of doped lanthanum gallate solid electrolyte with both the sintering temperature and the content of the minor phase, enhanced mechanical properties were obtained with the addition of 8YSZ to LSGM.

Table I - Values of reduced elastic modulus (REM) and hardness of LSGM, 8YSZ, 8YSZ10, and 8YSZ20 composites sintered at 1450 ºC.

Material	Load (mN)	REM (GPa)	Hardness (GPa)
LSGM	8	189±9	13.6±0.4
8YSZ	8	206±5	18.2±0.3
8YSZ10	8	216±2	15.1±0.3
8YSZ20 soft phase	8	212±1	14.6±0.5
8YSZ20 hard phase	8	217±5	15.5±0.2

CONCLUSIONS

Composite solid electrolytes constituted by doped lanthanum gallate ($La_{0.9}Sr_{0.1}Ga_{0.8}Mg_{0.2}O_{3-\delta}$, LSGM) and 8 mol% yttria-stabilized zirconia (8YSZ) were obtained by solid-state sintering. The lanthanum zirconate impurity phase was found in the 8YSZ20 composite (LSGM-20 wt% 8YSZ). The mean grain size of composites was lower than that of the matrix up to sintering temperatures of 1400 ºC. The line scan profile obtained by EDS revealed impurity phases due to the enrichment of magnesium, oxygen, and gallium at grain boundaries. The reduced elastic modulus and hardness of 8YSZ10 (LSGM-10 wt% 8YSZ) and 8YSZ20 were higher than that of the matrix.

ACKNOWLEDGMENTS

REFERENCES

[1] N.Q. Minh, J. Am. Ceram. Soc. **76** (1993) 563.

[2] T. Ishihara, H. Matsuda, Y. Takita, J. Am. Chem. Soc. **116** (1994) 3801.

[3] M. Feng, J.B. Goodenough, Eur. J. Solid State Inorg. Chem. **31** (1994) 663.

[4] T. Ishihara, H. Matsuda, Y. Takita, Solid State Ionics **79** (1995) 147.

[5] E. Djurado, M. Labeau, J. Eur. Ceram. Soc. **18** (1998) 1397.

[6] C. Oncel, B. Ozkaya, M.A. Gulgun, J. Eur. Ceram. Soc. **27** (2007) 599.

[7] N. Liu, M. Shi, C. Wang, Y.P. Yuan, P. Majewski, F. Aldinger, J. Mater. Sci. **41** (2006) 4205.

[8] R.H.L. Garcia, V. Ussui, N.B. Lima, E.N.S. Muccillo, D.R.R. Lazar, J. Alloys Compd. **486** (2009) 747.

[9] C.M. Fernandes, A. Castela, F.M. Figueiredo, J.R. Frade, Solid State Ionics **193** (2011) 52.

[10] G. Hao, X. Liu, H. Wang, H. Be, L. Pei, W. Su, Solid State Ionics **255** (2012) 81.

[11] M. Ghatee, Fuel Cells **18** (2018) 13.

[12] S.L. Yu, Z. Wang, L. Yang, J. Liu, R. Guan, Y. Xiao, T.M. He, J. Am. Ceram. Soc. **104** (2021) 329.

[13] J.J. Nie, D. Zheng, K.S. Ganesh, M. Akbar, C. Xia, W.J. Dong, X.Y. Wang, H. Wang, B.Y. Wang, Ceram. Int. **47** (2021) 3462.

[14] N. Porotnikova, A. Khrustov, A. Farlenkov, A. Khodimchuk, G. Partin, I. Ananyev, ACS Appl. Mater. Interfaces **14** (2022) 6180.

[15] W. Wei, N. Mushtaq, Y. Lu, M.A.K. Yousaf Shah, L. Ma, S. Yan, Crystals **13** (2023) 41.

[16] Y.-C. Wu, M.-J. Lee, X. Li, J. Eur. Ceram. Soc. **35** (2015) 4485.

[17] S. Xu, X.P. Lin, B. Ge, D. Ai, J. Ma, Z.J. Peng, Int. J. Appl. Ceram. Technol. **16** (2019) 108.

[18] T.G. Fujimoto, M.C. Steil, E.N.S. Muccillo, ECS Trans. **103** (2021) 2163.

[19] R. Pandey, P. Singh, A.K. Singh, P. Singh, Mater. Today Proc. **49** (2022) 3071.

[20] T.G. Fujimoto, S.L. Reis, E.N.S. Muccillo, Mater. Res. **22** (2019) e20190043.

[21] S.L. Reis, E.N.S. Muccillo, Ionics **24** (2018) 1693.

[22] M. Kleitz, J.H. Kennedy, in "Fast ion transport in solids, electrodes and electrolytes", P. Vashishta, J.H. Mundy, G.K. Shenoy (Eds.), North-Holland, Amsterdam (1979) 185.

[23] W.C. Oliver, G.M. Pharr, J. Mater. Res. **19** (2004) 3.

[24] Y.C. Wu, M.Z. Lee, Ceram. Int. **39** (2013) 9331.

[25] R. Muccillo, J. Mater. Res. **24** (2009) 1780.

[26] J.W. Stevenson, T.R. Armstrong, J.R. Pederson, J. Li, C.A. Levinshon, S. Baskaran, Solid State Ionics **113-115** (1998) 571.